Frontiers in Bioscience Landmark

Front. Biosci. (Landmark Ed) **2025**; 30(3): 27236
https://doi.org/10.31083/FBL27236

Original Research

Plasma Lipidomics, Gut Microbiota Profile, and Phenotype of Adipose Tissue in an *ApoE*$^{-/-}$ Mouse Model of Plaque Instability

Guanlin Yang[1,2,†], Xin Tan[2,†], Qiong Zhai[2], Yuewu Wang[3], Xuan Zhang[2], Pengwei Zhao[2], Fangyuan Liang[3], Jingkun Lu[2,*], LiLi Bao[2,*]

[1]Laboratory of Pharmacology, Zaozhuang Thoracic Hospital, 277500 Zaozhuang, Shandong, China
[2]School of Basic Medicine, Inner Mongolia Medical University, 010107 Hohhot, Inner Mongolia, China
[3]School of Pharmacy, Inner Mongolia Medical University, 010107 Hohhot, Inner Mongolia, China
*Correspondence: 20070123@immu.edu.cn (Jingkun Lu); baolili1203@126.com (LiLi Bao)
[†]These authors contributed equally.
Academic Editor: Rajesh Katare
Submitted: 30 October 2024 Revised: 12 January 2025 Accepted: 8 February 2025 Published: 21 March 2025

Abstract

Background: An appropriate animal model that can simulate the pathological process of atherosclerosis is urgently needed to improve treatment strategies. This study aimed to develop a new atherosclerosis model using *ApoE*$^{-/-}$ mice and to characterize lipidomics, gut microbiota profiles, and phenotypic alterations in adipose tissue using this model. **Methods**: After a 14- or 18-week high-fat diet (HFD), male *ApoE*$^{-/-}$ mice were randomly divided into four groups and treated separately with or without short-term and strong co-stimulation, including ice water bath and intraperitoneal injection of lipopolysaccharide and phenylephrine. As a control group, C57BL/6 mice were fed with conventional chow. The serum lipid levels, aortic arch pathology, adipose tissue phenotypic changes, plasma lipidomics, and *16S rDNA* gene sequencing of colon feces were investigated. **Results**: The serum lipid levels were significantly lowered following extended HFD feeding for four weeks. However, co-stimulation increased serum interleukin (IL)-1β levels but did not affect serum lipid profiles. Co-stimulation revealed typical vulnerable atherosclerotic plaque characteristics and defective adipose hypertrophy associated with peroxisome proliferator-activated receptor γ (PPARγ) regulation in adipose tissue and a reduction in mitochondrial uncoupling protein 1 (UCP1) within brown adipose tissue. Plasma lipidomic analysis showed that sphingomyelin (SM), ceramide (Cer), and monohexosylceramide (HexCer) levels in plasma were significantly elevated by HFD feeding, whereas co-stimulation further elevated HexCer levels. Additionally, glycerophosphocholines (16:0/16:0, 18:2/20:4, 18:1/18:1) and HexCer (C12:1, C16:0), Cer (d18:1/16:0), and SM (C16:0) were the most sensitive to co-stimulation. Combined co-stimulation and HFD-fed increased the abundance of *Firmicutes*, the abundance of *f_Erysipelotrichaceae*, and the *Firmicutes/Bacteroidota* ratio but decreased the abundance of microflora promoting bile acid metabolism and short-chain fatty acids (SCFAs) in mouse feces. The results were consistent with the findings of epidemiologic atherosclerotic cardiovascular disease studies. **Conclusions**: This study established an *ApoE*$^{-/-}$ mouse atherosclerotic vulnerable plaque model using a multi-index evaluation method. Adipogenic disorders, dysregulation of lipid metabolism at the molecular level, and increasing harmful gut microbiota are significant risk factors for vulnerable plaques, with sphingolipid metabolism receiving the most attention.

Keywords: atherosclerosis; vulnerable plaque; sphingolipid; gut microbiota; *ApoE*$^{-/-}$ mouse

1. Introduction

Atherosclerotic cardiovascular disease (ACVD) is a chronic, multi-factorial condition involving lipid metabolic disorders, chronic inflammation, vulnerable plaques, and a proclivity for vascular thrombosis, all of which are risk factors for the condition [1]. Continuous endothelial cell injury cause lipid deposition, platelet adhesion, and arterial smooth muscle cell proliferation, while vascular turbulence and low temperature damage accelerate plaque progression [2]. The initial stage of atherosclerosis involves lipid deposition in the arterial endothelium, ranging from lipid spots to lipid streaks. Smooth muscle cells then proliferate and migrate, and the number of circulating Ly6chi monocytes rises. Most of these cells are drawn into the plaque, becoming foam cells upon the additional absorption of oxidatively damaged lipoproteins [3,4]. In addition, bacteria-host interactions are closely linked to the initiation, progression, and repeated aggravation of atherosclerotic lesions, which may eventually result in thrombus formation, leading to acute coronary syndromes or stroke [5]. Pathological and imaging studies indicate that fragile plaques in human arteries show large necrotic cores, thinner or fractured fiber caps, more macrophages, spotted calcium, and positive remodeling [1,6,7].

Dysregulated lipid metabolism and gut microbiota dysbiosis are two established risk factors for ACVD [8–10]. Recent advances in coronary artery disease lipidomics have demonstrated that particular lipids, including oxidized lipids, sphingomyelin (SM) with its long saturated fatty acyl chains, glycerophosphocholines (PCs) with its saturated and monounsaturated heavy acyl chains, ceramide (Cer), and monohexosylceramide (HexCer, a subclass of gluco-

sylceramide), are linked to the clinical classification and features of coronary artery disease [8,9,11–13]. In addition, lipopolysaccharides (LPSs) are known to be integral proteins of gram-negative bacteria that regulate the development of atherosclerosis. In one study, 516 middle-aged people participated in a five-year epidemiological study, and those with plasma LPS concentrations of 50 g/mL or higher had a three-fold greater risk of developing atherosclerosis than those with lower levels [8]. The catecholamine neurotransmitter phenylephrine is a vasoconstrictor that significantly increases plaque rupture rates [10]. Furthermore, numerous studies have demonstrated a connection between the gut microbiota and the development of atherosclerosis. A high-fat diet (HFD) is known to disrupt the balance of the gut microbiota, contributing to the progression of cardiovascular diseases by increasing the abundance of Erysipelotrichaceae, facultative anaerobes, and opportunistic pathogens [14].

White, beige, and brown adipocytes moderate metabolic health in humans. Accompanied by adipocytes and immune cells (such as B cells, T cells, and macrophages), white adipose tissue (WAT) stores excess energy and regulates endocrine functions. Brown adipose tissue (BAT), a type of thermogenic adipose tissue, is multilocular, is enriched in mitochondria, and exhibits high levels of the mitochondrial uncoupling protein 1 (UCP1), which controls thermogenesis and energy metabolism. Adipose tissue dysfunction associated with chronic inflammation has been identified as a cause of atherosclerosis. Gutiérrez-Cuevas *et al.* (2021) [15] reported that visceral WAT dysfunction increases the levels of pro-inflammatory adipokines, oxidative stress, and the renin-angiotensin-aldosterone system, leading to myocardial fibrosis and cardiac dysfunction. In another study, the association between BAT and cardiometabolic diseases was retrospectively analyzed in 52,487 study participants, and individuals with higher BAT/weight ratios independently correlated with lower odds of coronary artery disease, cerebrovascular disease, and other metabolic diseases, supported by lower values of blood glucose, triglycerides, and high-density lipoprotein levels [16].

Numerous atherosclerosis (AS) models have been constructed to induce the formation of atherosclerotic plaques using different methods [17], including physical injury [18], pharmacological action, and gene knockout approaches [19,20]. However, these atherosclerosis models pathologically represent some, but not all, features of ruptured human plaques [17,18,21]. For both primary and clinical research, a suitable animal model of human ruptured plaques is essential, considering the limits of clinical studies on mechanism mining. Therefore, this study was conducted to establish an *ApoE*$^{-/-}$ murine model of atherosclerotic plaque instability to investigate alterations during the intermediate and advanced stages of atherosclerosis. As triggers for the ruptured plaques, a HFD and short-term co-stimulation (including LPS, phenylephrine intraperitoneal injection, and cold exposure) were employed. A set of indices for model evaluation was developed based on serum biochemical indicators and descriptions of pathomorphological alterations in plaques. Plasma lipidomics, gut microbiota composition, and adipose tissue phenotype were evaluated after 14 weeks and 18 weeks of HFD-fed with or without co-stimulation. Furthermore, levels of peroxisome proliferator-activated receptor γ (PPARγ) expression related to adipogenesis regulation and the serum inflammatory cytokine interleukin (IL)-1β were determined. It was anticipated that the molecular basis for human plaque rupture and new disease management strategies could be determined using this model.

2. Materials and Methods

2.1 Animals and Treatments

Male *ApoE*$^{-/-}$ (8 weeks old; 20–24 g) and wildtype C57BL/6 (8 weeks old, 22–25 g) mice were purchased from SiPeiFu BioTech Co., Ltd. (Beijing, China) and housed in an environment with a 12-h light cycle, controlled temperature (21–24 ℃), and free access to water and food. After *ApoE*$^{-/-}$ mice were fed an HFD (BEIJING KEAO XIELI Co., Ltd., # D12079B, Beijing, China) containing 21% fat, 50% carbohydrate, and 20% protein for 14 or 18 weeks, a modified mixture of short-term stimuli at the end of the experiment was used to activate unstable plaques, as reported by Wang *et al.* [19]. The mice undergoing short-term co-stimulation were divided into Model B-14wks (n = 12) and Model B-18wks (n = 12) groups. Specifically, after 14 or 18 weeks of HFD, mice in Model B groups were treated with short-term stimuli, including an iced water bath (0 °C) for 5–10 min on day 1 and 2, intraperitoneal injection with 1 µg/kg/day of LPS on day 1 and 2, and then intraperitoneal injection with 8 µg/kg of phenylephrine on day 3 (Fig. 1A). The *ApoE*$^{-/-}$ mice fed with HFD without co-stimulation were divided into "Model A-14wks" (n = 10) and "Model A-18wks" (n = 9). C57BL/6 mice (n = 10) served as the control group and were fed a standard chow diet (3% calories from fat). Body weight and food intake were recorded weekly for all mice.

2.2 Tissue Collection and Processing

After 12 h of fasting, the mice were sacrificed under 5% isoflurane inhalation anesthesia and blood samples, the heart's aortic root, the entire aorta, BAT on the scapular surface, and epididymal white adipose tissue (eWAT) were harvested for follow-up analysis.

2.3 Measurement of Serological Parameters

Serum total triglyceride (TG), total cholesterol (TC), low-density lipoprotein cholesterol (LDL), and high-density lipoprotein cholesterol (HDL) levels were measured using commercially accessible kits (Nanjing Jiancheng Bioengineering Institute, A110-1-1, A111-1-1, A113-1-

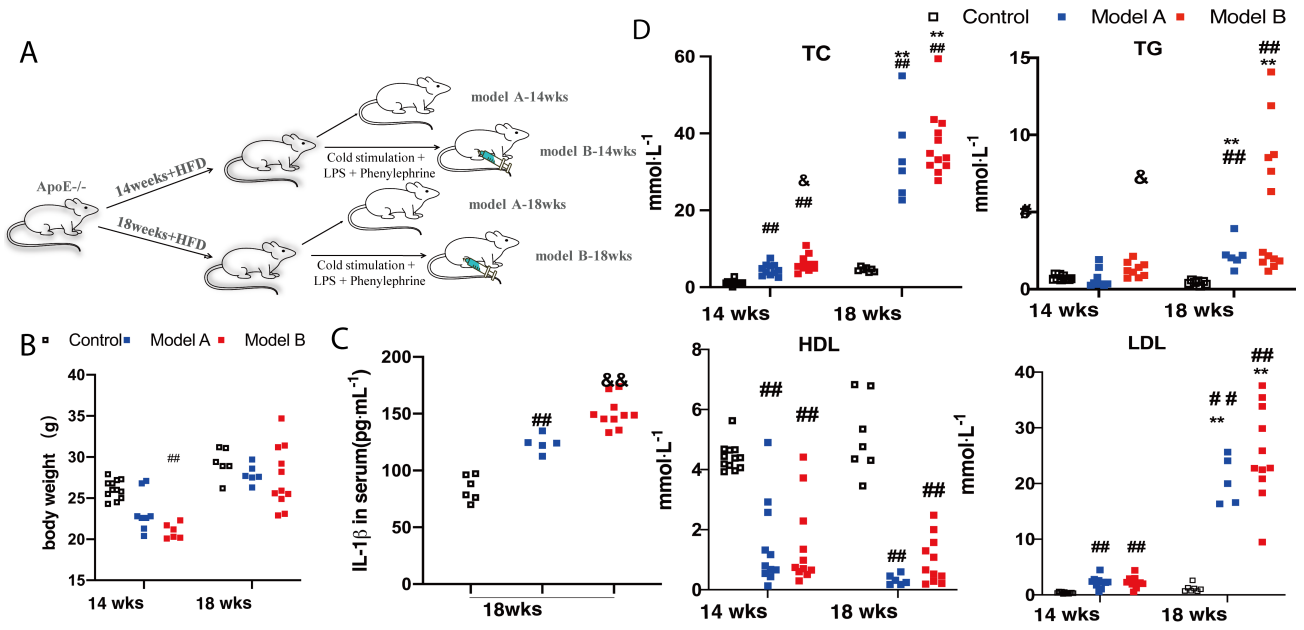

Fig. 1. Body weight and biochemical parameters of mice. (A) Experimental procedure. (B) Body weight of mice at 14 and 18 weeks. (C) Serum interleukin (IL)-1β levels at 18 weeks. (D) Total cholesterol (TC), triglyceride (TG), low-density lipoprotein (LDL), and high-density lipoprotein (HDL) levels at 14 and 18 weeks. $^{\#\#}p < 0.01$ vs. the control group at the same period. $^{**}p < 0.01$ vs. the corresponding model group at 14 weeks. $^{\&}p < 0.05$ vs. Model A at the same period. $^{\&\&}p < 0.01$ vs. Model A at the same period.

1, A112-1-1, Nanjing, Jiangsu, China). Mouse IL-1β was determined using enzyme-linked immunosorbent assay (ELISA) kits (DAKEWE Biotech Co., Ltd., 1210122, Shenzhen, China).

2.4 Histological Analysis

2.4.1 Determination and Evaluation of Atherosclerosis

Necrotic core formation is a hallmark of unstable atherosclerotic plaques. The unstable necrotic core is a pit of hypocellular plaque lacking collagen and containing thin fibrous caps, necrotic debris, and cholesterol clefts. During the progression of atherosclerosis, the major arterial vessels undergo outward remodeling, thereby increasing the lumen area. When evaluating atheroma lesions, the area occupied by atherosclerotic lesions was measured via en face Oil Red O staining of the aorta, and the degree of severity was quantified as the percentage of atherosclerotic lesion area corrected by the total aortic volume. Following a gradient of 10%, 20%, and 30% sucrose-saturated solutions for dehydration, the heart's aortic root embedded in the optimal cutting temperature (OCT) medium was cut into 7-µm serial sections. Hematoxylin and eosin (H&E) staining was used to analyze the areas of plaques, necrotic cores, and vascular cross-sections [22]. The plaque compositions of lipids, collagens, smooth muscle cells (SMC), and macrophages were evaluated using Oil Red O (Service, #G2013, Wuhan, China) staining, Masson's three-color stain (Solarbio, #G1340, Beijing, China), immunohistochemistry for the anti-α-smooth actin (SMA) Rabbit pAb (1:200; Service, #GB111364, Wuhan, China), and anti-F4/80 Rabbit pAb (1:200; Service, #GB113373, Wuhan, China), respectively. A plaque stability score formula was established: plaque stability score = (macrophage area + lipid region)/(SMC area + collagen region), as described in the literature [7,23].

2.4.2 Histological Analysis of Adipose Tissue

The adipose tissue was embedded in paraffin wax, sliced to 5-µm thickness, stained using a H&E kit (Service bio, G1076, Wuhan, China), and then photographed under an optical microscope (Leica, DM3000, Wetzlar, Germany).

2.5 Plasma Lipidomic Analysis

Liquid-liquid-mass spectrometry (LC-MS) technology is the foundation of lipidomic research [24,25]. Lipidomic analysis was analyzed at Novogene Technology Co., Ltd. (Beijing, China). Vortex treatment was performed on a 100 µL plasma sample (IAS) mixed with 750 µL methanol. Subsequently, at room temperature (21–24 °C), 2.5 mL of methyl tertiary butyl ether (MTBE) was added, and the mixture was shaken for 1 h. Phase separation was induced by adding 0.625 mL of MS-grade water, followed by a 10-min incubation. The samples were then centrifuged for 10 min at 1000 *g*. The upper phase was collected, while the lower phase underwent a second extraction using 1 mL of a solvent mixture (MTBE:methanol:water = 10:3:2.5, v/v/v). The organic phases from both extractions were combined, dried, and stored at –80 °C for no longer than 3 months. Be-

fore analysis, the dried residue was re-dissolved in 100 µL of isopropanol. Quality control (QC) samples were prepared by pooling and equilibrating aliquots from each plasma sample. Plasma lipidomic ultra-high-performance liquid chromatography coupled to tandem mass spectrometry (UHPLC-MS/MS) analysis was conducted using a high-field quadrupole orbitrap (Q Exactive™ HF-X) mass spectrometer system (Thermo Fisher Scientific Inc., Dreieich, Germany), coupled with a Thermo Vanquish™ UHPLC system (Thermo Fisher Scientific Inc., Dreieich, Germany), equipped with a heated electrospray ionization interface (ESI) (UHPLC-Q-Exactive-MS/MS analysis). Chromatographic separation was performed on a Thermo Accucore C30 (2.1 × 150 mm, 2.6 µm) chip (Thermo Fisher Scientific Inc., Dreieich, Germany). Data were captured and analyzed using Xcalibur 3.1 (Thermo Fisher Scientific Inc., Dreieich, Germany). The column temperature was set at 40 °C, the flow rate was 0.35 mL/min, and the injection volume was 5 µL. The mobile phase consisted of phases A (acetonitrile/H_2O, 6/4) and B (isopropanol/acetonitrile, 1/9) containing 0.1% formic acid and 10 mM ammonium acetate in a 20 min gradient detection as follows: 30% B, initial; 30% B, 2 min; 43% B, 5 min; 55% B, 5.1 min; 70% B, 11 min; 99% B, 16 min; 30% B, 18.1 min [26]. Analyses were performed in both positive and negative ionic modes. The operating parameters were optimized as follows: sheath gas, 20 arbitrary units; sweep gas, 1 arbitrary unit; auxiliary gas rate, 5 for positive mode and 7 for negative mode; spray voltage: 3 kV; capillary temperature: 350 °C; heater temperature: 400 °C; S-Lens Radio Frequency (RF) level: 50; automatic gain control target: 10^6; normalized collision energy: 25, 30 for positive mode and 20, 24, and 28 for negative mode; injection time: 100 ms; isolation window: 1 m/z; automatic gain control target (MS_2): 10^5; dynamic exclusion: 15 s, and a mass range recorded at 114–1700 m/z. The raw data were imported into the Compound Discoverer 3.01 (CD3.1, Thermo Fisher Inc., Dreieich, Germany) for preliminary screening. The parameters were set: *Rt* deviation of 0.2 min; m/z deviation of 5 ppm; signal strength deviation of 30%; a signal-to-noise ratio of 3, minimum signal intensity of 10^5; and peak extraction of information such as addition ions. Subsequently, the peak area was quantified, and the target ions were integrated. The molecular ion peaks and fragmentation ions predicted the molecular formula. This was then compared with Lipidmaps (https://lipidmaps.org) and Lipid Blast databases (https://fiehnlab.ucdavis.edu/projects/LipidBlast). Blank samples were used to remove background interference. Quantitative results were obtained after normalizing data.

2.6 Gut Microbiota Analysis

Fecal samples for *16S rDNA* gene sequencing were analyzed at Novogene Technology Co., Ltd. (Beijing, China). Community DNA fragments underwent paired-end sequencing using the Illumina HiSeq PE250 platform (NovaSeq6000, San Diego, CA, USA). The bioinformatics pipeline for microbiome analysis was implemented in QIIME 2 (https://qiime2.org). Amplification of the V3–V4 regions of the *16S rRNA* gene was achieved with the specific primers *F515* (5′-CACGGTCGKCGGCGCCATT-3′) and *R806* (5′-GGACTACHVGGGTWTCTAAT-3′), using the gg_13 database (https://www.arb-silva.de/) and DADA2 (https://benjjneb.github.io/dada2/) as the primary denoising method. Experimental data reliability was evaluated through rarefaction and species accumulation curves. Species diversity within samples was assessed with α-diversity indices (Chao1 and Shannon), while β-diversity measures, including Principal Coordinate Analysis (PCoA) were used to examine inter-sample variation. A series of statistical analyses (*T*-test, MetagenomeSeq, and linear discriminant analysis effect size [LEfSe]) were performed to determine the difference in community structure. Differential metabolites were defined as those meeting the criteria of variable importance in projection (VIP) >1, $p < 0.05$, and fold change (FC) ≥ 2 or FC ≤ 0.5.

2.7 Western Blotting

Frozen adipose tissue samples were homogenized for 30 min with radioimmunoprecipitation buffer (1% phenylmethylsulfonyl fluoride (PMSF)). In addition, protein expression levels of PPARγ (1:1000; Proteintech, #16643-1-AP, Wuhan, Hubei, China) and glyceraldehyde 3-phosphate dehydrogenase (GAPDH) (1:2000; Service, #GB12002, Wuhan, China) were determined using western blotting methods.

2.8 Statistical Analyses

Image-Pro Plus6.0 software (Media Cybernetics, Rockville, MD, USA) was used to analyze histopathological images. Statistical analyses were conducted with GraphPad Prism 9.0 (GraphPad Software, San Diego, CA, USA), and the results were expressed as mean ± SD. To assess statistical significance, a two-way analysis of variance (ANOVA) and an unpaired two-tailed Student's *t*-test were utilized, with $p < 0.05$ considered significant. Partial least squares discriminant analysis (PLS-DA) was performed using SIMCA 14.1 software (Sartorius Stedim Data Analytics, Uppsala, Sweden), and hierarchical clustering analysis (HCA) was performed using R-language heat map packages (https://cran.r-project.org). Differential metabolites were identified based on VIP >1, $p < 0.05$, and a FC ≥ 2 or ≤ 0.5. Pathway analyses of significantly different metabolites were performed using the MetaboAnalyst 5.0 (https://www.metaboanalyst.ca), and the pathways having impact values $>$–0.05 and –log(p) $>$ –2 were analyzed.

3. Results

3.1 Deterioration in Biochemical Parameters With Prolonged HFD in ApoE$^{-/-}$ Mice

The weights of the mice and serum biochemical parameters were analyzed to determine the effect of the combined intervention and HFD on serum lipid levels. In contrast to the weight of mice in the control group at 14 weeks, the weight of mice in the Model B-14wks group was reduced (Fig. 1B) ($p < 0.01$), and the serum TC and TG levels were significantly higher than those in the Model A-14wks group (Fig. 1D) ($p < 0.01$). As expected, the serum TC, TG, and LDL levels were significantly increased in the Model A-18wks and Model B-18wks groups compared to those in the Model A-14wks and Model B-14wks groups and the HDL levels were decreased (Fig. 1D) ($p < 0.01$).

Notably, at 18 weeks, the serum IL-1β level was noticeably higher in the two Model groups than in the control group, while the IL-1β level was significantly higher in the Model B-18wks group than in the Model A-18wks group (Fig. 1C) ($p < 0.01$). The results showed that consuming a HFD for a longer period increased blood lipid and IL-1β levels; co-stimulation did not affect the serum lipid levels but lowered the mouse body weight at 14 weeks and further exacerbated inflammation at 18 weeks, suggesting that the effect of cold stimulation in a mouse model demonstrates time-dependent characteristics. At week 14, cold stimulation effectively promoted heat production in the adipose tissue of mice, thereby increasing overall metabolism, which may have subsequently led to weight loss. However, by week 18, this heat-producing capacity of adipose tissue decreased significantly, appearing to lose its previous metabolic function. This variation suggests that adipose tissue exhibits distinct responses to cold stimulation during different developmental stages, potentially impacting weight management and energy metabolism in mice.

3.2 Co-Stimulation Decreased Plaque Stability

The results of Oil Red O staining of the en face of the whole aorta are shown in Fig. 2A. With short-term co-stimulation, the ratio of plaque area to the aorta (the positive region of Oil Red O staining) was significantly higher in the two model groups at 18 weeks than in the corresponding groups at 14 weeks ($p < 0.05$, $p < 0.01$), and the rise in the ratio in the Model B-18wks group was more significant than that in the Model B-14wks group ($p < 0.01$). Oil O staining of the aortic sinus slices revealed a similar result (Fig. 2B), showing a larger ratio of Oil O staining area to plaque area in Model B mice than in Model A mice during the same period ($p < 0.01$).

H&E staining of the transverse aortic sinus was utilized to assess the cross-sectional vessel area, the plaque-to-vessel area ratio, and the necrotic core-to-plaque area ratio. The collagen content was evaluated using Masson's trichrome staining. A damaged fibrous cap and erythrocyte accumulation layer indicated previous rupture and healing processes [11]. As shown in Fig. 3A,B, when *ApoE*$^{-/-}$ mice were fed the HFD and co-stimulated, a substantially greater plaque-to-vascular area ratio was observed in the Model B group than in the Model A group at the same period ($p < 0.05$). Accordingly, the percentage of necrotic cores was the largest, or they had even ruptured in Model B-18wks mice, and the cross-sectional vessel area was significantly larger in model mice at 18 weeks than in those at 14 weeks ($p < 0.05$) (**Supplementary Fig. 1**). In addition, Masson staining (Fig. 3C) showed that the collagen fibers in the Model B-14wks, Model B-18wks, and Model A-18wks groups were fewer and sparser than those in the Model A-14wks group ($p < 0.01$).

To quantify the contents of macrophages and smooth muscle cells in aortic plaques, immunohistochemical staining was performed using F4/80 and α-SMA as specific markers, respectively. The results revealed no change in the percentage of F4/80-positive area to plaque area between the groups and a significant decrease in the rate of α-SMA (Fig. 3D,E). The vulnerability index of plaques in Model B-18wks mice was the highest and was 1.5-fold higher than that in Model B-14wks and Model A-18wks mice and 3.6-fold higher than that in Model A-14wks mice ($p < 0.05$, $p < 0.01$), as shown in Fig. 3F.

These results suggest that a prolonged HFD promotes abnormal arterial vessel dilation and the rupture of elastic fibers. Furthermore, short-term co-stimulation accelerated lipid deposition onto the vessels, forming sparser, more extensive, and vulnerable plaques in the short term. The plaque phenotype observed in Model B-18wks mice was similar to that of unstable human plaques [27], including a huge plaque size, necrotic core, thin fibrous cap, decrease in entirety collagen, and positive remodeling, that is, a significant increase in vessel area. As the HFD time increased, these characteristics became more pronounced.

3.3 Co-Stimulation Altered the Adipose Tissue Phenotype

In the case of an excess energy supply, WAT causes adipocyte hypertrophy (increase in volume) or hyperplasia (increase in number). During adipose tissue remodeling, hyperplasia of WAT is generally more advantageous than adipocyte hypertrophy. This is because small adipocytes exhibit increased insulin sensitivity compared with large adipocytes, whereas large adipocytes often indicate metabolic derangements [28,29]. In this study, the adipocyte phenotype in mice was assessed (Fig. 4). With co-stimulation, the size of eWAT adipocytes in Model B-18wks mice was severely increased compared to that of Model B-14wks mice (Fig. 4A), and the BAT adipocytes in Model B mice showed widespread hypertrophy both at 14 and 18 weeks in comparison to those of Model A at the same period (Fig. 4B). In addition, the ratio of both eWAT and BAT to body weight (mg/g) of model mice at 18 weeks was higher than that of the corresponding mice at 14 weeks ($p < 0.01$, or $p < 0.05$) (Fig. 4C).

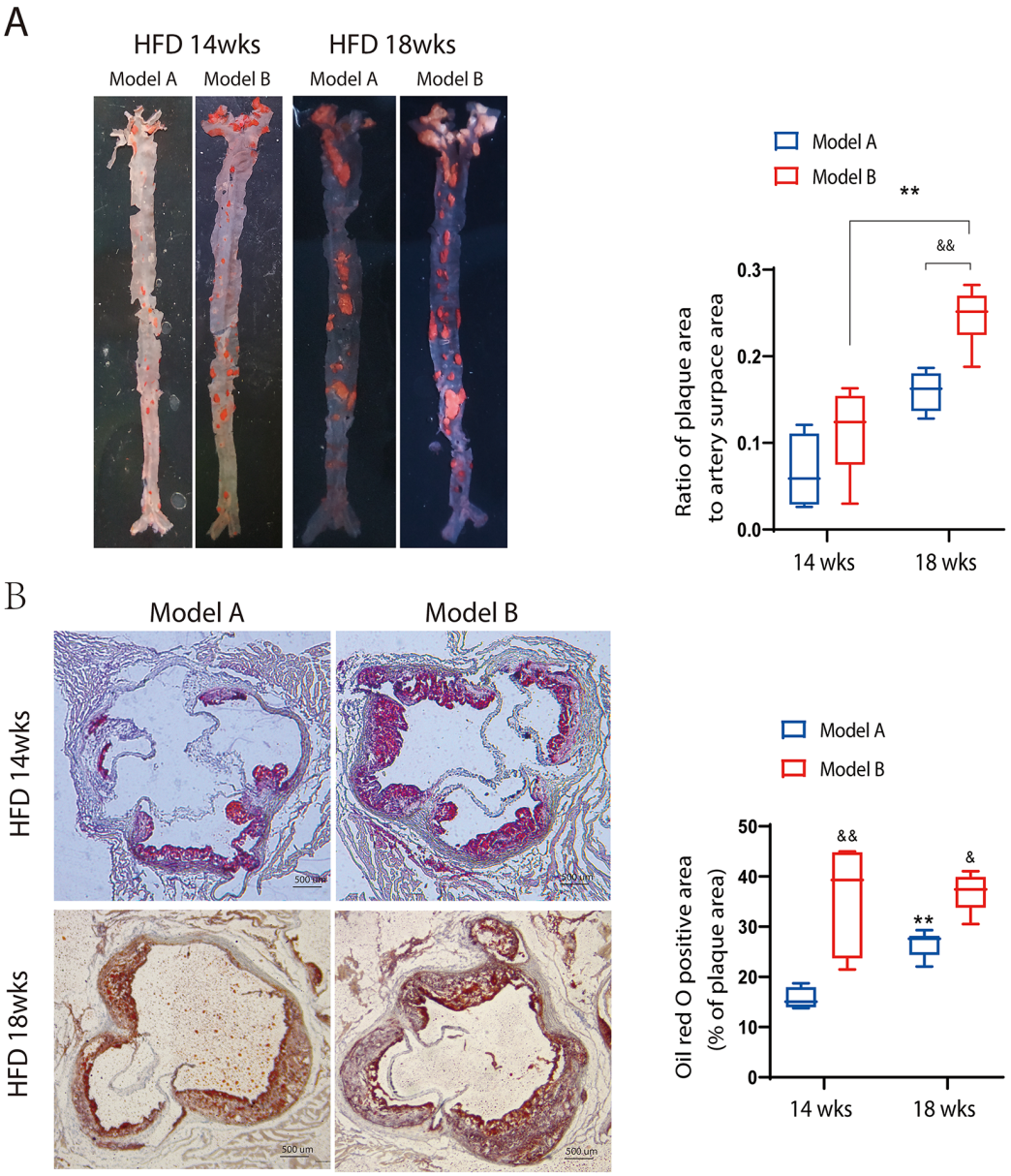

Fig. 2. Oil red O staining of the face of the whole aorta and cross-sections of the aortic sinus. (A) Oil red O staining of the whole aorta. (B) Oil red O staining of the aortic sinus. Scale bar: 500 µm. $^{**}p < 0.01$, vs. the corresponding model group at 14 weeks, $^{\&}p < 0.05$, $^{\&\&}p < 0.01$ vs. Model A at the same period, n = 6. HFD, high-fat diet.

PPARγ, a transcription factor, is highly expressed in adipocytes and is the critical regulator of adipogenesis. It also regulates lipid and glucose homeostasis. Several studies have demonstrated the inhibitory role of PPARγ in atherosclerosis [30]. The results showed that co-stimulation effectively reduced PPARγ expression in eWAT and BAT at 18 weeks compared to controls. In contrast, PPARγ expression in the eWAT of Model A-18wks mice significantly increased (Fig. 4D). These findings suggest that co-stimulation did not affect total body weight, but it was more likely to cause further adipocyte hypertrophy than hyperplasia, especially in eWAT, by attenuating PPARγ expression in HFD-fed mice.

3.4 Co-Stimulation Altered the Plasma Lipidomics Profile

Plasma samples from each group at 18 weeks were analyzed using UHPLC-Q-Exactive-MS/MS under both electrospray lonization (ESI) positive and negative ion modes. To maintain data reliability, QC samples were included in the sequence, which was run after every seven injections. The Pearson correlation coefficient between QC samples was between 0.99 and 1, indicating that the method was stable and appropriate for these samples throughout the testing process. Typical base peak ion chromatograms are shown in **Supplementary Fig. 2**. To minimize false positives, we further screened the data according to Skotland *et al.* [31]. A total of 988 lipid molecules was iden-

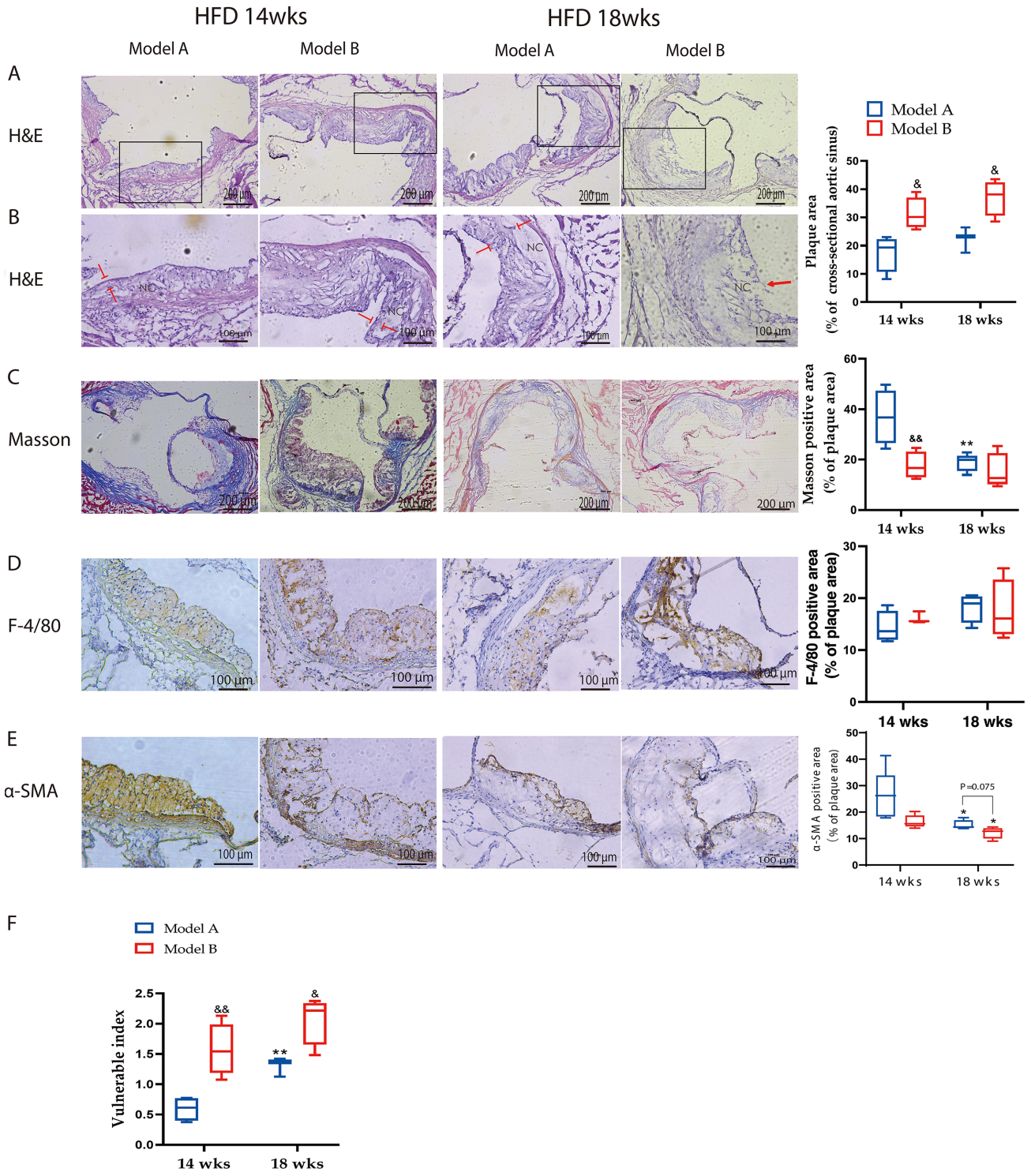

Fig. 3. Plaque characteristics of *ApoE*$^{-/-}$ mice after combined stimulation. (A) H&E staining of the aortic sinus of Model A and B mice fed with an HFD after 14 or 18 weeks. The box shows a substantially greater plaque-to-vascular area ratio was observed in the Model B group than in the Model A group at the same period ($p < 0.05$). (B) Local swelling showing the necrotic cores (NC) or plaque rupture. The red arrows point to the fibrous cap. (C) Masson's trichrome staining. (D) α-SMA immunostaining. (E) F4/80 immunostaining. Scale bar: 200 μm (A), 100 μm (B), 200 μm (C), 100 μm (D), 100 μm (E). (F) Vulnerable plaque index = (macrophage area + lipid area)/(smooth muscle cells (SMC) area + collagen area). Model A mice were only fed an HFD. Model B mice were treated with an HFD plus combined stimulation, including ice water (0 °C, not submerged) for 5–10 min/time/day and intraperitoneal injection of 1.0 μg/kg/day lipopolysaccharide (LPS) for 2 days, followed by 8.0 μg/kg phenylephrine on day. $^{**}p < 0.01$, $^{*}p < 0.05$ vs. the corresponding model group at 14 weeks, $^{\&}p < 0.05$, $^{\&\&}p < 0.01$ vs. Model A at same period, n = 6.

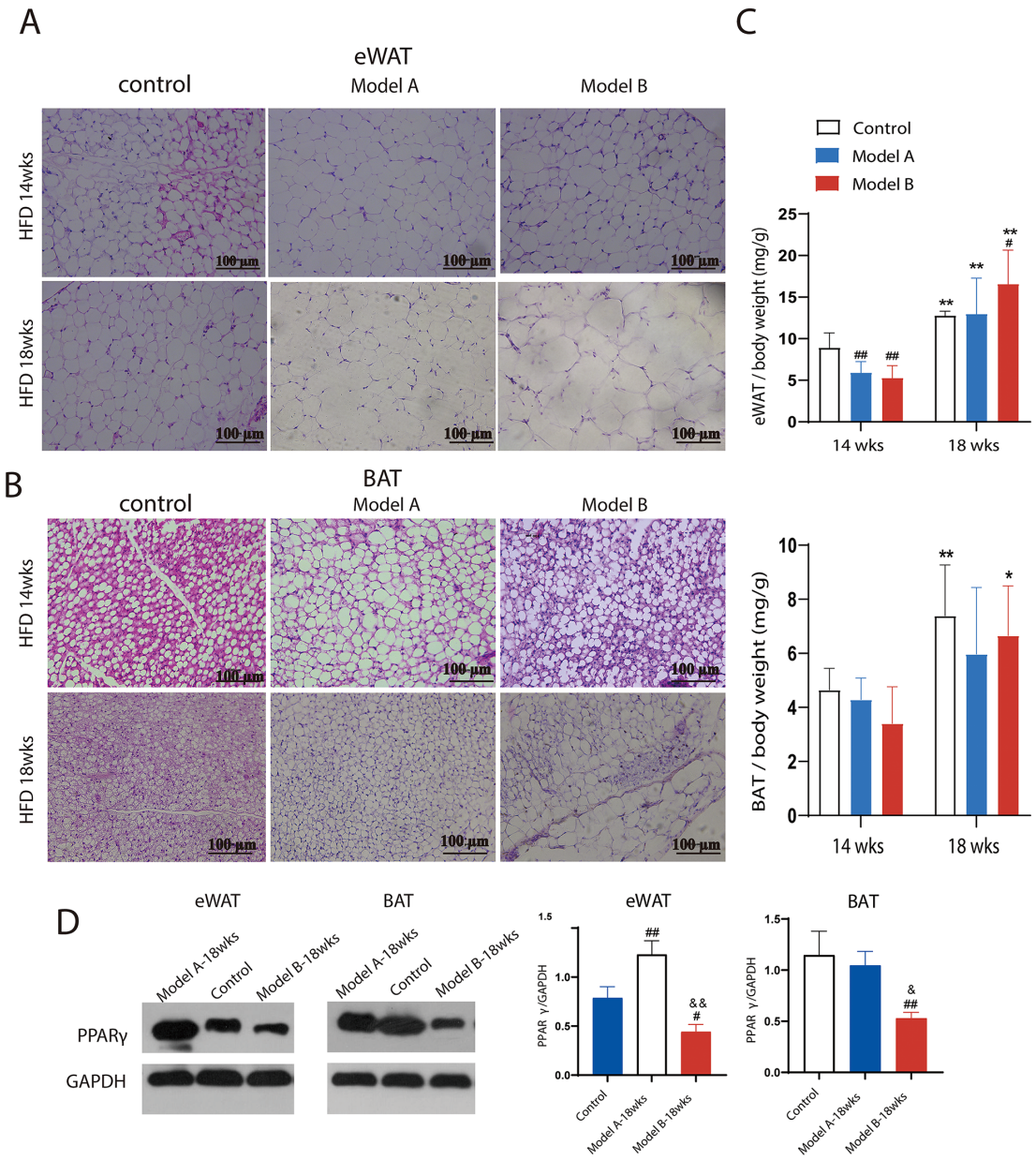

Fig. 4. Combined treatment altered adipose tissue phenotype. (A) H&E staining of white epididymal tissue (eWAT), n = 4–6. (B) H&E staining of brown adipose tissue (BAT), n = 4–6. (C) Ratio (mg/g) of BAT and eWAT to body weight, n = 10. (D) Peroxisome proliferator-activated receptor γ (PPARγ) protein of BAT and eWAT of mice subjected to western blotting, glyceraldehyde 3-phosphate dehydrogenase (GAPDH) was used as a loading control, n = 3. $^{\#\#}p < 0.01$, $^{\#}p < 0.05$ vs. Control group at same period, $^{*}p < 0.05$, $^{**}p < 0.01$ vs. the corresponding model group at 14 weeks, $^{\&}p < 0.05$, $^{\&\&}p < 0.01$ vs. Model A at the same period. Scale bar: 100 μm.

tified and analyzed, and these were mainly grouped into 16 subclasses, including fatty acyl (FA), triacylglycerols, PC, phosphatidylethanolamine, phosphatidylserine, phosphatidylglycerol, phosphatidic acid, phosphatidylinositol, SM, Cer, and HexCer. Detailed information about the identified lipids is presented in **Supplementary Fig. 3**.

Heatmaps of HCA and PLS-DA plots were used to visualize the cluster overview of all plasma samples from the Model A-18wks, Model B-18wks, and control groups having significantly different lipid compositions (Fig. 5A and **Supplementary Fig. 4**). The volcano plot analysis results revealed that the plasma lipid compositions of Models B and A at 18 weeks were notably altered compared to those of the control group; that is, more than 400 molecules were upregulated, and 30 molecules were downregulated in both groups (**Supplementary Fig. 5**). The apparent separation between Model A-18wks and Model B-18wks is shown in Fig. 5B, with good model quality (R2: 0.69 and Q2: –0.78 in positive ion modes; R2: 0.76 and Q2: –0.68 in negative ion modes, respectively; $p < 0.05$). The above results sug-

gest that the lipid metabolism disorders were more severe following combined stimulation with HFD than with HFD alone.

In line with recent studies [7–10], the statistical significance of the plasma lipid variables was determined using PLS-DA based on the criteria of VIP >1, FC >1.5, FC <0.67, and $p < 0.05$. The most striking changes occurred in specific lipid subclasses (Fig. 5C). Compared to the control, the ratios (%) of the peak area of Cer, SM, and HexCer to the total plasma lipids significantly increased in both model groups and PC, FA (–54%), and phosphatidylinositol (–29%) were reduced in the Model B-18wks group. Only a slight increase in the HexCer (+34%) ratio was observed in the Model B-18wks group compared with that in the Model A-18wks group ($p < 0.05$, $p < 0.01$), indicating that upregulation of Cer, SM, and HexCer levels was closely related to the atherosclerotic characteristics caused by HFD (Fig. 5D). In contrast, a further increase in HexCer levels may be more closely related to the vulnerability of plaques induced by co-stimulation in HFD-fed mice. Cer, SM, and HexCer belong to sphingolipid subclasses. Numerous studies have demonstrated that sphingolipids participate in atherosclerosis development and progression [32]. Ceramides have also been linked in recent research to adipocyte malfunction that underlies metabolic disorders [33]. According to the enrichment analysis, this study revealed that co-stimulation mainly impacted the sphingolipid metabolic pathway (Fig. 5E) by regulating Cer, SM, and HexCer metabolism.

To determine the potential lipid markers linked to AS plaque vulnerability, individual molecules showing significant differences were analyzed. Compared with those in the control and Model A-18wks group, 19 lipid components were significantly elevated in the Model B-18wks group ($p < 0.01$ or $p < 0.05$), including PC (18:0e/20:1, 16:1/18:1, 18:0e/20:3, 22:3e/18:0, 22:5e/20:5), SM (d14:1/18:0, 14:1/26:0, d18:1/22:0), Hexosylceramide-N-Dihydrosphingosine (HexCer-NDS) (d20:0/12:1, d18:0/16:0, d28:0/12:1), Hexosylceramide-N-Sphingosine (HexCer-NS) (d18:2/16:0, d18:1/22:0, d18:2/22:0, d28:1/12:1, d20:2/20:0, d22:1/12:1), and glycerophosphoethanolamine (PE) (16:0/20:0, 20:0/18:1) ($p < 0.01$ or $p < 0.05$), as shown in Fig. 5D. The results suggest that these lipid components may influence plaque stability.

Several clinical cohort trials [9,13] have confirmed that multiple individual lipid components, including Cer (d18:1/16:0, d18:1/18:0, and d18:1/24:1), HexCer (d18:1, d18:2, C16–C18, C20–C26), SM-16, and PC (16:0/16:0, 16:0/18:1, 18:0/16:1), are positively associated with the risk of cardiovascular disease (CVD) outcomes, while lysophosphatidylcholine (LPC) (16:0, 18:0, 18:1, 18:2, and 20:4) is inversely correlated [34]. Additionally, Chen *et al.* [35] analyzed plasma lipidomics in C57BL/6J mice on a normal diet, C57BL/6J mice, and $ApoE^{-/-}$ mice on a 16-week HFD; after controlling for the effects of the HFD, they found that reductions in C16 sphingosine and PC (17:1/22:6) levels and increases in PC (18:2/20:4), PC (16:0/16:0), PC (18:0/16:1), SM (d18:1/24:1), SM (d16:0/28:5), and SM (d18:1/16:0) levels were positively associated with AS. Therefore, we further assessed these reported cardiovascular risk markers. Notably, 17 lipid species were consistent with the clinical studies, given that Cer-NS (d18:1/16:0, d18:1/24:1, and d18:1/24:0), HexCer-NS (d18:1/16:0), SM (d14:1/16:0 and d26:3/16:0), and PC (16:0/16:0, 16:0/18:1, 18:0/18:1, 18:1/18:1, and 18:4e/18:1) levels were significantly higher, while LPC (18:2, 18:0, 16:0, 20:4) and PC (18:2/20:4) levels were significantly lower in the two model groups than in the control group ($p < 0.01$ or $p < 0.05$). Moreover, only PCs (18:0/18:1) were significantly higher in the Model B-18wks group than in the Model A-18wks group ($p < 0.05$ or $p < 0.01$) (Fig. 5F). These observations suggested that co-stimulation further exacerbated lipid metabolism disorders in mice fed an HFD and that PC (16:0/16:0, 18:2/20:4, 18:1/18:1), HexCer (C12:1, C16:0), Cer (d18:1/16:0), SM (C16:0), and SM containing long chains of saturated fatty acids may be markers of the risk of vulnerable plaque formation. The sphingolipid metabolic pathway is crucial in the progression and formation of atherosclerotic plaques.

3.5 Combined Stimulation Altered the Intestinal Flora

Using 16S rRNA sequencing of the colon contents, we examined the effects of long-term HFD and short-term co-stimulation on the intestinal microbiota of $ApoE^{-/-}$ mice. The results are shown in Fig. 6A, where the operational taxonomic unit rarefaction curve is seen to gradually flatten as the sequencing volume increases, indicating adequate sequencing data. Compared with the control group, the results of α-diversity (Fig. 6B) showed increases in the richness (chao1 index) and diversity (Shannon index) of microbial communities in the Model B-18wks group (Shannon: $p = 0.061$). PCoA and orthogonal PLS-DA were performed to observe the β-diversity of the microbial communities (Fig. 6C,D). The results demonstrated a partial overlap between the control and Model A-18wks groups. However, the microbial communities showed clear segregation between the Model A-18wks and Model B-18wks groups, demonstrating that co-stimulation notably altered the gut microbiota composition.

Subsequently, the community composition and species abundance were examined across various taxonomic levels. At the phylum level (Fig. 7A,B), the Model B-18wks group had significantly greater levels of dangerous bacteria (*p_Firmicutes*) and significantly lower relative abundances of beneficial bacteria (*p_Bacteroidota*) compared to the Model A-18wks groups ($p < 0.05$ or $p < 0.01$), resulting in a considerably higher ratio of *p_Firmiciutes to p_Bacteroidoa* (F/B) in the Model B-18wks group than in the other two groups ($p < 0.05$). Additionally, differences

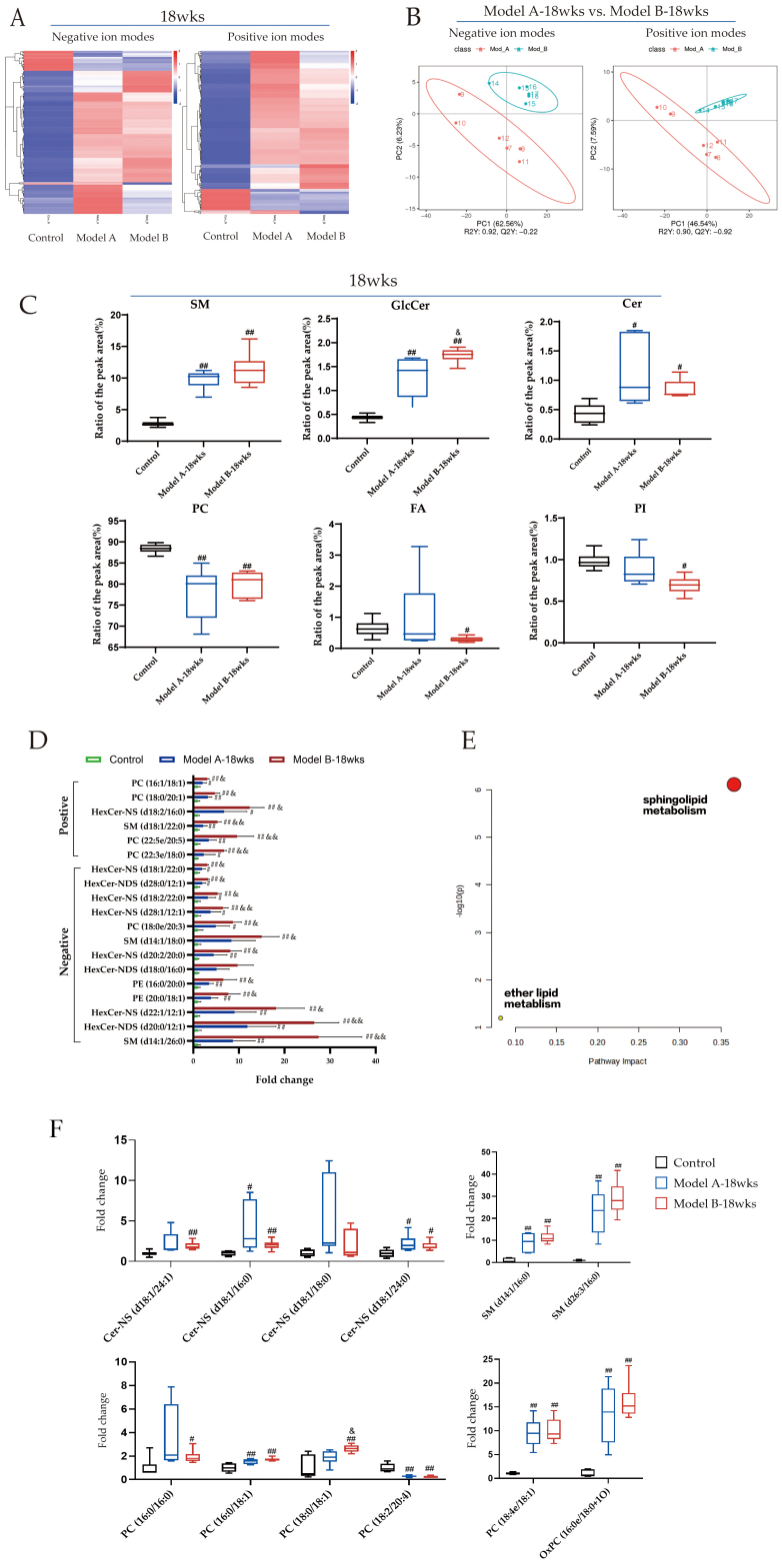

Fig. 5. Co-stimulation altered plasma lipidomic profiles. (A) Clustering heat maps of hierarchical clustering analysis (HCA) between three groups. (B) Partial least squares discriminant analysis (PLS-DA) score plot of Model A-18wks vs. Model B-18wks group. (C) Ratio of the peak area of lipid subclasses to the plasma lipid (%). (D) Potential lipid markers associated with plaque vulnerability were assessed using the thresholds of variable importance in projection (VIP) >1.4 compared with the control group, and fold change (FC) >1.5 or FC <0.5 compared with the Model A-18wks group, area $>10^7$, and $p < 0.05$, n = 6. (E) Pathway analysis of significantly different metabolites, impact value >0.05 and –log(p) > 2. (F) Several cardiovascular risk markers reported in some clinical studies were evaluated, $^{\#\#}p < 0.01$, $^{\#}p < 0.05$ vs. Control group, $^{\&}p < 0.05$, $^{\&\&}p < 0.01$ vs. Model at the same period.

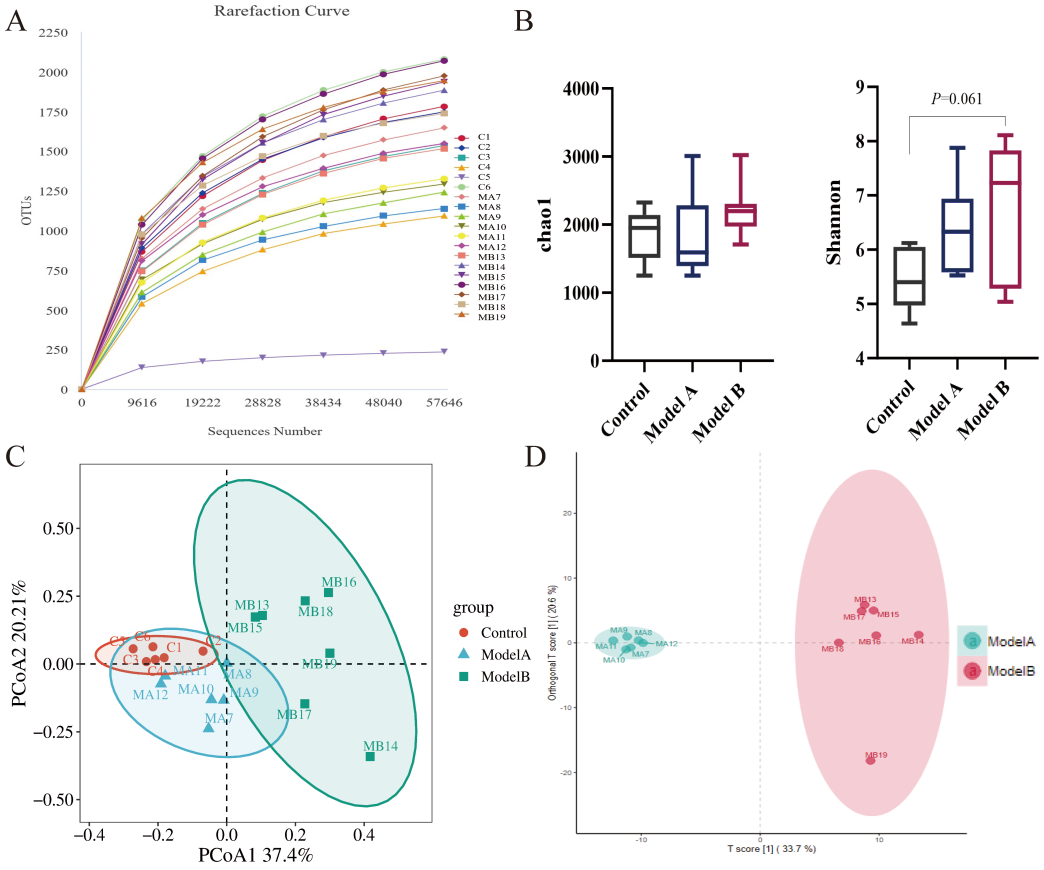

Fig. 6. Combined stimulation increases intestinal microflora disorders. (A) Operational taxonomic unit rarefaction curve. (B) Chao1 and Shannon indices reflect the α-diversity of the gut microbiota. Data are presented as mean $\pm$ SD. (C) Principal Coordinate Analysis (PCoA) analysis reflects β-diversity. (D) Orthogonal PLS-DA analysis between the Model A and Model B groups.

in microbiota composition were visualized using LEfSe and clustering heatmap analysis. Fig. 7C,D show the relative abundance of microbiota clustering heatmaps of the TOP10 at the family level and TOP30 at the genus level, respectively. These heatmaps reveal that the changes at the family and genus levels were more significant in the Model B-18wks group than in the Model A-18wks group. Based on similar trends in both model groups, compared with the control group, the representative differential bacteria ($p < 0.05$) in the Model B-18wks group are shown in Fig. 7E. Of these, the abundances of *f_Muribaculaceae*, *f_Lachnospiraceae*, *g_Family_XIII_UCG-001* [14,36], which promotes the formation of short-chain fatty acids (SCFAs), and *g_Muribaculum* [37], which maintains intestinal homeostasis, were significantly reduced. The Model B-18wks group showed significant increases in *f_Erysipelotrichaceae*, *g_Faecalibaculum* [14], *f_Peptostreptococcaceae*, *f_Bifidobacteriaceae* [14], *g_Romboutsia* [38], *g_Clostridium_sensu_stricto_1* [14] abundance. These harmful bacteria are positively correlated with high-fat and high-sugar diets, obesity, dyslipidemia, or enteritis. With linear discriminant analysis (LDA) >3.5, the LEfSe analysis results from the phylum to the species level are shown in Fig. 7F,G. Compared with the control group, both model groups showed an increased abundance of *g_Faecalibaculum* and a decreased abundance of beneficial bacteria such as *g_Ileibacterium*, *s_Ileibacterium_valens* [39,40], which are involved in bile acid metabolism. Thus, co-stimulation with HFD further enhanced the abundance of harmful bacteria associated with abnormal glycolipid metabolism and lowered the abundance of beneficial bacteria promoting SCFA and comparing bile acid metabolism to HFD alone. The stability of atherosclerotic plaques may be affected by the changes in their abundance.

4. Discussion

To reproduce the risk of coronary artery disease in humans, we employed short-term stimulation (with a combination of LPS, phenylephrine injection, and cold) to trigger atherosclerotic plaque rupture in HFD-fed *ApoE*$^{-/-}$ mice. HDF-fed *ApoE*$^{-/-}$ mice with stimulation had higher TC, TG, and LDL levels, lower HDL levels, and enhanced atherosclerotic plaque growth than HDF-fed *ApoE*$^{-/-}$ ones. Although brief co-stimulation did not appreciably affect blood lipid levels, it resulted in significant vulner-

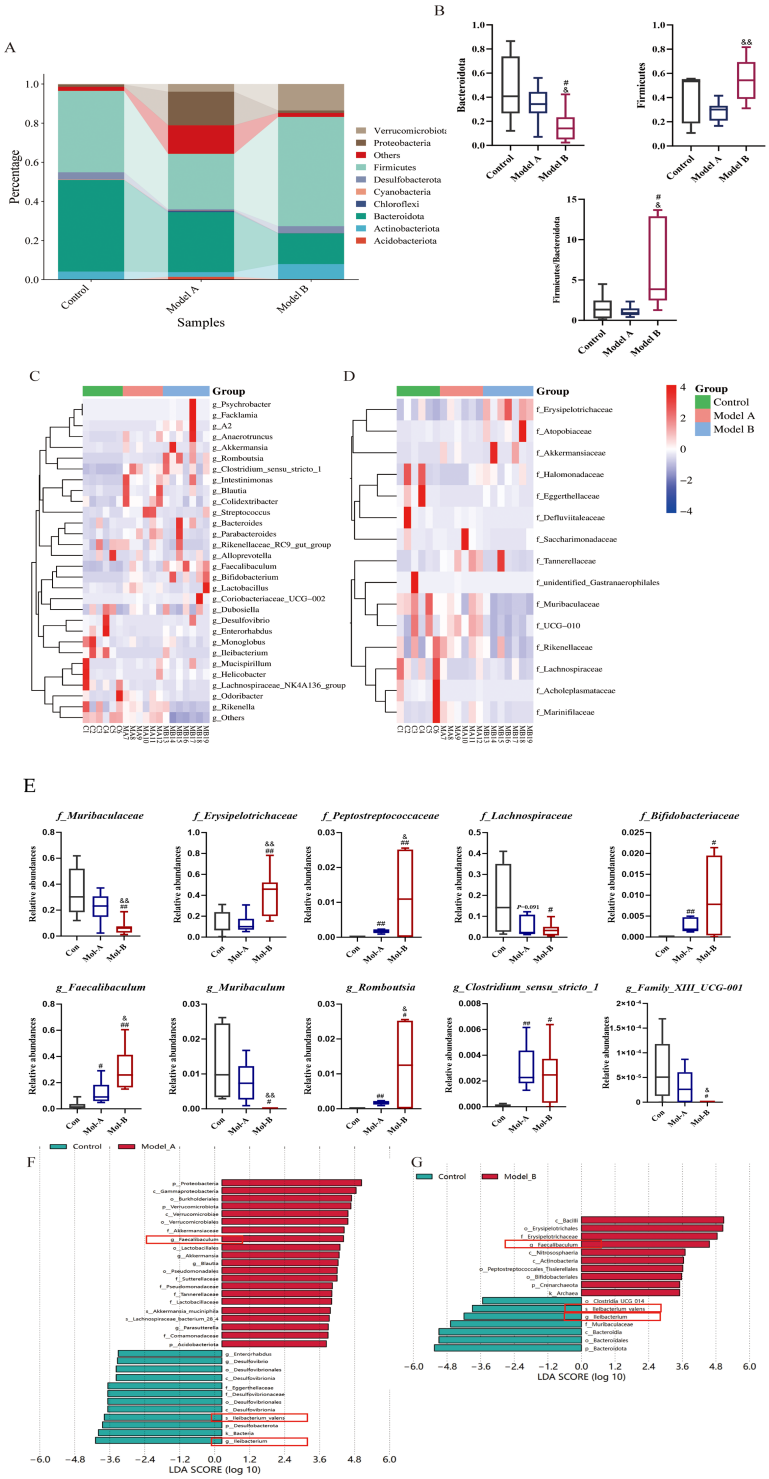

Fig. 7. Combined stimulation alters the dominant microflora composition from the phylum to the species level. (A) Stacked chart of microbial flora at the phylum level. (B) Relative abundance of *Firmicutes* and *Bacteroidota* and the ratio of *Firmiciutes* to *Bacteroidota* (*F/B*). Data are presented as mean ± SD. (C) HCA heatmap of microbial flora at the family level. (D) HCA heatmap of microbial flora at the genus level. (E) Representative differential microflora at the family and genus levels. $^{\#}p < 0.05$ vs. control group, $^{\#\#}p < 0.01$ vs. control group, $^{\&\&}p < 0.01$, $^{\&}p < 0.05$ vs. Model A-18wks group, n = 6. (F) Linear discriminant analysis effect size (LEfSe) from the phylum to species level between the control and Model A-18wks groups. Linear discriminant analysis (LDA) >3.5. (G) LEfSe from the phylum to species level between the control and Model B-18wks groups. LDA >3.5. The red boxes in (F,G) highlight key bacterial taxa with significant differences in both two model groups, compared with the control group.

ability to atherosclerotic plaques. Specifically, the model involving co-stimulation and a HFD for 18 weeks exhibited many vulnerable plaque characteristics [41], including an increased vessel area, large plaque size, necrotic core, increased lipid accumulation, a thin or disrupted/buried fibrous cap, decreased total collagen, increased expansion of macrophage cells, decreased SMCs, and increased plaque vulnerability index. Simultaneously, Multilayered subsurface fibrous caps and erythrocyte extravasation were observed in some samples, suggesting prior plaque rupture and subsequent neointimal healing.

Lipid metabolic abnormalities are a hallmark of atherosclerosis, which is a chronic illness. Adipose tissue dysfunction can induce dyslipidemia, activate vascular inflammation, and promote atherosclerosis development [42]. Our study revealed that a HFD markedly increased the adipose tissue-to-body weight ratio (mg/g), adipocyte hyperplasia, and high PPARγ expression in eWAT. In contrast, co-stimulation resulted in increased and defective adipose hypertrophy related to lower PPARγ expression in adipose tissue, primarily in the 18-week WAT.

Lipidomics analysis has the potential for false positives, due to the complexities involved in lipid extraction and characterization. Variability in sample preparation and ionization efficiency can lead to misidentification of lipid species, potentially skewing results. Experts in the field, Skotland *et al*. (2024) [31], suggested some simple guidelines for assessing the likelihood of lipid species being present. These guidelines for mammalian samples include ① Major lipid species should not contain fatty acyl chains or long-chain bases with an odd number of carbon atoms; ② The major fatty acyl chains in phospholipids and glycerolipids contain 16–22 carbon atoms with minor amounts of C14; ③ Fatty acyl chains of sphingolipids typically contain 14–26 carbon atoms with no or only one double bond; ④ In glycosphingolipids, the double bond is found mainly in fatty acyl chains with 22 carbons or higher. In this study, the data was chosen and examined using the aforementioned standards.

Sphingolipids consist primarily of the most abundant SM (approximately 87%), complex HexCer (9–10%), and Cer (approximately 3%) in human plasma. In a retrospective subcohort (n = 5991) of the LIPID study, higher total Hex-Cers were associated with a significantly higher CVD risk, with HexCer (d18:1/16:0) and HexCer (d18:1/18:0) as high-risk markers [34]. Another study [13] analyzed the plasma lipids of 2627 Singaporeans of Chinese heritage and found that total Cer levels were not associated with CVD risk. However, higher levels of circulating HexCer, total long chain sphingolipids (C16–C18), and complete 18:1 sphingolipids were associated with an increased CVD risk. A few plaque samples from patients who died from atherosclerosis revealed a significant increase in HexCer levels in the intima tissue where the plaque grows compared with those in areas without plaque [43]. These findings reveal that HexCer, similar to Cer, is a high-risk lipid marker for CVDs. Certain sphingolipid species are associated with atherogenesis. Particular attention has been paid to the association between phospholipids and CVD. Accumulation of Cer species is observed in atherosclerotic lesions and obesity and is strongly correlated with diabetes; certain types of Cer species have emerged as predictive biomarkers for future cardiovascular adverse events [44]. In this study, the lipidomics results revealed an apparent elevation of SM, Cer, and HexCer levels induced by HFD, and additional upregulation of HexCer in the lipid composition caused by co-stimulation, revealing the most vital relationship between HexCer species and plaque vulnerability. In addition, analysis of the individual lipid molecules revealed that PC (16:0/16:0, 18:2/20:4, 18:1/18:1), HexCer (C12:1, C16:0), Cer (d18:1/16:0), SM (C16:0), and SM containing long saturated fatty acyl chains may be risk markers for vulnerable plaques.

Mounting evidence suggests that plaque stability may be greatly impacted by the complex crosstalk between HexCer, PPAR signaling, SCFA metabolism, and adipose tissue dysfunction [45,46]. Elevated levels of HexCer have been associated with insulin resistance and chronic inflammation in adipose tissue, factors that are pivotal in the progression of metabolic disorders and cardiovascular diseases [47]. Furthermore, Jang *et al*. [48] reported that HexCer increased rosiglitazone-induced PPARγ activation and adipogenesis in WAT by directly interacting with PPARγ via the A/B domain, suggesting that the effect of HexCer on plaque stability may be related to PPARγ expression in adipose tissue.

As bacteria metabolites, SCFAs are essential for adipose tissue metabolism and anti-atherosclerosis. By controlling the gut microbiota, SCFAs trigger fatty acid oxidation and glycolysis [49]. Yi *et al*. [50] reported that SCFAs can significantly inhibit oxidized low-density lipoprotein (Ox-LDL)-induced macrophage activation and inflammatory damage by modulating the NOD-, LRR- and pyrin domain-containing protein 3 (NLRP3) Caspase-1 signaling pathway, suggesting that Exogenous SCFAs, by regulating immune responses and cellular metabolism, may provide new therapeutic targets for atherosclerosis. Wang *et al*. [51] reported that SCFAs altered the distribution of the lipid in serum and inhibited adipogenic differentiation by suppressing the function of Cers and further decreasing PPARγ expression in adipose tissues of pigs. The expression of the lipolytic gene (hormone-sensitive lipase, HSL) and the abundance of Cers are associated with the production and functions of SCFAs in the gut [51]. Additionally, SCFAs upregulate PPARγ and PPARα, which are involved in adipocyte differentiation and energy expenditure. SCFAs are negatively correlated with atherosclerosis and are beneficial for plaque stabilization [52]. Emoto *et al*. [53] found that the proportion of *Firmicutes/Bacteroidetes* in patients with coronary CVD was increasing. In this

study, combined stimulation further increased *Firmicutes* abundance and the *F/B* ratio and decreased the microflora that promote bile acid metabolism and SCFAs in HFD-fed mice. In particular, combined stimulation caused the disappearance of *g_Family_XIII_UCG-001*, which is negatively correlated with acute cardiovascular events [54]. Atherosclerotic plaque stability can be affected by the abundance of *g_Faecalibaculu*, *f_Peptostreptococcaceae*, *g_Romboutsia*, *g_Romboutsia*, *s_Ileibacterium_valens*, *g_Muribaculum,* and *g_Family_XIII_UCG-001*.

Increased amounts of circulating lipids deposited in non-adipose tissues, such as the heart and blood vessel walls, result from metabolic abnormalities in adipose tissue that impact circulating lipid metabolism [55]. A compelling body of evidence suggests that Cers may be responsible for a significant portion of tissue damage in various cardiometabolic disorders. Furthermore, HexCer accumulation is positively correlated with the number of macrophages in plaques, and it induces the release of pro-inflammatory cytokines such as tumor necrosis factor (TNF)-α and monocyte chemoattractant protein (MCP)-1 [32]. In this study, the model mouse plaques showed significant vulnerability characteristics similar to those of vulnerable plaques in clinical patients. In addition, the levels of Cer and HexCer plasma lipids increased significantly, and BAT and eWAT were abnormally hypertrophied. These features are consistent with literature reports [56–58]. However, further research is required to determine the link between phenotypic changes in adipocytes and macrophages, intestinal flora, and Cer metabolism in this model.

5. Conclusions

A novel *ApoE*$^{-/-}$ model was developed using short-term co-stimulation plus 18 weeks of HFD. The results demonstrated that atherosclerotic plaque vulnerability, adipogenesis disorders, lipid metabolic inflexibility, and harmful microflora increases were similar to those in middle- to late-stage atherosclerosis. This study lays the groundwork for further scientific research and the development of associated drugs. It is evident that Cer and HexCer metabolism can aggravate atherosclerosis progression and increase inflammatory responses; however, to elucidate the underlying mechanisms, further research is required to determine how HexCer is linked to adipose tissue dysfunction, SCFA metabolism, and the PPAR pathway.

Abbreviations

HFD, high-fat diet; Cer, ceramide; HexCer, monohexosylceramide; LPC, lysophosphatidylcholine; SM, sphingomyelin; CVD, cardiovascular disease; IL, interleukin; TC, total cholesterol; TG, triglyceride; SCFA, short-chain fatty acid; WAT, white adipose tissue; BAT, brown adipose tissue; QC, quality control; PLS-DA, partial least square discriminant analysis; SMA, smooth actin; LDL, low-density lipoprotein; HDL, high-density lipoprotein; LPS, lipopolysaccharide; HCA, hierarchical clustering analysis; FC, fold change; LEfSe, linear discriminant analysis effect size; H&E, hematoxylin and eosin; FA, fatty acyl; PPARγ, peroxisome proliferation-activated receptor γ; AS, atherosclerosis; PC, glycerophosphocholine; PE, glycerophosphoethanolamine; Ox-LDL, oxidized low-density lipoprotein; PCoA, Principal Coordinate Analysis.

Availability of Data and Materials

The original contributions presented in the study are included in the article/Supplementary Material, further inquiries can be directed to the corresponding author.

Author Contributions

Conceptualisation, JL, and LB; Data curation, GY, QZ, and FL; Funding acquisition, JL; Methodology, JL, YW, and GY; Investigation and Validation, PZ, and XZ; Visualization, GY, QZ; Writing an original draft, GY; Writing review and data curation, XT. All authors contributed to editorial changes in the manuscript. All authors have read and agreed to the published version of the manuscript. All authors have participated sufficiently in the work and agreed to be accountable for all aspects of the work.

Ethics Approval and Consent to Participate

The animal study was reviewed and approved by the Biomedical Ethics Committee of Inner Mongolia Medical University (No. YKD2019146). All experiments were performed following the Animal Ethics Code and Operational Guidelines. All efforts were made to minimize animal suffering and discomfort in compliance with the 3R principles.

Acknowledgment

In addition to acknowledging peer reviewers' contributions for their thoughts and recommendations, we would like to thank everyone who assisted us in writing this paper.

Funding

This research was funded by the National Natural Science Foundation of China (grant no.81960757, 82260813).

Conflict of Interest

The authors declare no conflict of interest.

Supplementary Material

Supplementary material associated with this article can be found, in the online version, at https://doi.org/10.31083/FBL27236.

References

[1] Arbab-Zadeh A, Fuster V. From Detecting the Vulnerable Plaque to Managing the Vulnerable Patient: JACC State-of-the-Art Review. Journal of the American College of Cardiol-

ogy. 2019; 74: 1582–1593. https://doi.org/10.1016/j.jacc.2019.07.062.

[2] Libby P, Ordovas JM, Auger KR, Robbins AH, Birinyi LK, Dinarello CA. Endotoxin and tumor necrosis factor induce interleukin-1 gene expression in adult human vascular endothelial cells. The American Journal of Pathology. 1986; 124: 179–185.

[3] Mahdinia E, Shokri N, Taheri AT, Asgharzadeh S, Elahimanesh M, Najafi M. Cellular crosstalk in atherosclerotic plaque microenvironment. Cell Communication and Signaling. 2023; 21: 125. https://doi.org/10.1186/s12964-023-01153-w.

[4] Wang S, Wang X, Lv Y, Zhang Z, He T, Hao X, *et al*. M2 Macrophage-Derived Exosomes Inhibit Atherosclerosis Progression by Regulating the Proliferation, Migration, and Phenotypic Transformation of Smooth Muscle Cells. Frontiers in Bioscience (Landmark Edition). 2024; 29: 288. https://doi.org/10.31083/j.fbl2908288.

[5] Chen L, Ishigami T, Doi H, Arakawa K, Tamura K. Gut microbiota and atherosclerosis: role of B cell for atherosclerosis focusing on the gut-immune-B2 cell axis. Journal of Molecular Medicine. 2020; 98: 1235–1244. https://doi.org/10.1007/s00109-020-01936-5.

[6] Shioi A, Ikari Y. Plaque Calcification During Atherosclerosis Progression and Regression. Journal of Atherosclerosis and Thrombosis. 2018; 25: 294–303. https://doi.org/10.5551/jat.RV17020.

[7] Lu W, Park SH, Meng Z, Wang F, Zhou C. Deficiency of Adipocyte IKKβ Affects Atherosclerotic Plaque Vulnerability in Obese LDLR Deficient Mice. Journal of the American Heart Association. 2019; 8: e012009. https://doi.org/10.1161/JAHA.119.012009.

[8] Ding M, Rexrode KM. A Review of Lipidomics of Cardiovascular Disease Highlights the Importance of Isolating Lipoproteins. Metabolites. 2020; 10: 163. https://doi.org/10.3390/metabo10040163.

[9] Kohno S, Keenan AL, Ntambi JM, Miyazaki M. Lipidomic insight into cardiovascular diseases. Biochemical and Biophysical Research Communications. 2018; 504: 590–595. https://doi.org/10.1016/j.bbrc.2018.04.106.

[10] Shen X, Li L, Sun Z, Zang G, Zhang L, Shao C, *et al*. Gut Microbiota and Atherosclerosis-Focusing on the Plaque Stability. Frontiers in Cardiovascular Medicine. 2021; 8: 668532. https://doi.org/10.3389/fcvm.2021.668532.

[11] Chatterjee S, Bedja D, Mishra S, Amuzie C, Avolio A, Kass DA, *et al*. Inhibition of glycosphingolipid synthesis ameliorates atherosclerosis and arterial stiffness in apolipoprotein E-/- mice and rabbits fed a high-fat and -cholesterol diet. Circulation. 2014; 129: 2403–2413. https://doi.org/10.1161/CIRCULATIONAHA.113.007559.

[12] Phinikaridou A, Andia ME, Shah AM, Botnar RM. Advances in molecular imaging of atherosclerosis and myocardial infarction: shedding new light on in vivo cardiovascular biology. American Journal of Physiology. Heart and Circulatory Physiology. 2012; 303: H1397–410. https://doi.org/10.1152/ajpheart.00583.2012.

[13] Seah JYH, Chew WS, Torta F, Khoo CM, Wenk MR, Herr DR, *et al*. Plasma sphingolipids and risk of cardiovascular diseases: a large-scale lipidomic analysis. Metabolomics. 2020; 16: 89. https://doi.org/10.1007/s11306-020-01709-8.

[14] Chen J, Xiao Y, Li D, Zhang S, Wu Y, Zhang Q, *et al*. New insights into the mechanisms of high-fat diet mediated gut microbiota in chronic diseases. iMeta. 2023; 2: e69. https://doi.org/10.1002/imt2.69.

[15] Gutiérrez-Cuevas J, Sandoval-Rodriguez A, Meza-Rios A, Monroy-Ramírez HC, Galicia-Moreno M, García-Bañuelos J, *et al*. Molecular Mechanisms of Obesity-Linked Cardiac Dysfunction: An Up-Date on Current Knowledge. Cells. 2021; 10: 629. https://doi.org/10.3390/cells10030629.

[16] Becher T, Palanisamy S, Kramer DJ, Eljalby M, Marx SJ, Wibmer AG, *et al*. Brown adipose tissue is associated with cardiometabolic health. Nature Medicine. 2021; 27: 58–65. https://doi.org/10.1038/s41591-020-1126-7.

[17] Matoba T, Sato K, Egashira K. Mouse models of plaque rupture. Current Opinion in Lipidology. 2013; 24: 419–425. https://doi.org/10.1097/MOL.0b013e3283646e4d.

[18] Noonan J, Bobik A, Peter K. The tandem stenosis mouse model: Towards understanding, imaging, and preventing atherosclerotic plaque instability and rupture. British Journal of Pharmacology. 2022; 179: 979–997. https://doi.org/10.1111/bph.15356.

[19] Wang Y, Johnson JA, Fulp A, Sutton MA, Lessner SM. Adhesive strength of atherosclerotic plaque in a mouse model depends on local collagen content and elastin fragmentation. Journal of Biomechanics. 2013; 46: 716–722. https://doi.org/10.1016/j.jbiomech.2012.11.041.

[20] Wang X, Fu Y, Xie Z, Cao M, Qu W, Xi X, *et al*. Establishment of a Novel Mouse Model for Atherosclerotic Vulnerable Plaque. Frontiers in Cardiovascular Medicine. 2021; 8: 642751. https://doi.org/10.3389/fcvm.2021.642751.

[21] Perazza LR, Mitchell PL, Jensen BAH, Daniel N, Boyer M, Varin TV, *et al*. Dietary sucrose induces metabolic inflammation and atherosclerotic cardiovascular diseases more than dietary fat in LDLr$^{-/-}$ApoB$^{100/100}$ mice. Atherosclerosis. 2020; 304: 9–21. https://doi.org/10.1016/j.atherosclerosis.2020.05.002.

[22] Ma T, Gao Q, Zhu F, Guo C, Wang Q, Gao F, *et al*. Th17 cells and IL-17 are involved in the disruption of vulnerable plaques triggered by short-term combination stimulation in apolipoprotein E-knockout mice. Cellular & Molecular Immunology. 2013; 10: 338–348. https://doi.org/10.1038/cmi.2013.4.

[23] Dong LH, Li L, Song Y, Duan ZL, Sun SG, Lin YL, *et al*. TRAF6-Mediated SM22α K21 Ubiquitination Promotes G6PD Activation and NADPH Production, Contributing to GSH Homeostasis and VSMC Survival In Vitro and In Vivo. Circulation Research. 2015; 117: 684–694. https://doi.org/10.1161/CIRCRESAHA.115.306233.

[24] Dunn WB, Broadhurst D, Begley P, Zelena E, Francis-McIntyre S, Anderson N, *et al*. Procedures for large-scale metabolic profiling of serum and plasma using gas chromatography and liquid chromatography coupled to mass spectrometry. Nature Protocols. 2011; 6: 1060–1083. https://doi.org/10.1038/nprot.2011.335.

[25] Want EJ, Wilson ID, Gika H, Theodoridis G, Plumb RS, Shockcor J, *et al*. Global metabolic profiling procedures for urine using UPLC-MS. Nature Protocols. 2010; 5: 1005–1018. https://doi.org/10.1038/nprot.2010.50.

[26] Narváez-Rivas M, Zhang Q. Comprehensive untargeted lipidomic analysis using core-shell C30 particle column and high field orbitrap mass spectrometer. Journal of Chromatography A. 2016; 1440: 123–134. https://doi.org/10.1016/j.chroma.2016.02.054.

[27] Vaisar T, Hu JH, Airhart N, Fox K, Heinecke J, Nicosia RF, *et al*. Parallel Murine and Human Plaque Proteomics Reveals Pathways of Plaque Rupture. Circulation Research. 2020; 127: 997–1022. https://doi.org/10.1161/CIRCRESAHA.120.317295.

[28] Haylett WL, Ferris WF. Adipocyte-progenitor cell communication that influences adipogenesis. Cellular and Molecular Life Sciences. 2020; 77: 115–128. https://doi.org/10.1007/s00018-019-03256-5.

[29] Liu W, Li D, Cao H, Li H, Wang Y. Expansion and inflammation of white adipose tissue - focusing on adipocyte progenitors. Biological Chemistry. 2020; 402: 123–132. https://doi.org/10.1515/hsz-2019-0451.

[30] Yin L, Wang L, Shi Z, Ji X, Liu L. The Role of Peroxisome Proliferator-Activated Receptor Gamma and Atherosclerosis:

Post-translational Modification and Selective Modulators. Frontiers in Physiology. 2022; 13: 826811. https://doi.org/10.3389/fphys.2022.826811.

[31] Skotland T, Ekroos K, McDonald J, Ahrends R, Liebisch G, Sandvig K. Pitfalls in lipid mass spectrometry of mammalian samples - a brief guide for biologists. Nature Reviews. Molecular Cell Biology. 2024; 25: 759–760. https://doi.org/10.1038/s41580-024-00758-4.

[32] Piccoli M, Cirillo F, Ghiroldi A, Rota P, Coviello S, Tarantino A, *et al*. Sphingolipids and Atherosclerosis: The Dual Role of Ceramide and Sphingosine-1-Phosphate. Antioxidants. 2023; 12: 143. https://doi.org/10.3390/antiox12010143.

[33] Li Y, Talbot CL, Chaurasia B. Ceramides in Adipose Tissue. Frontiers in Endocrinology. 2020; 11: 407. https://doi.org/10.3389/fendo.2020.00407.

[34] Mundra PA, Barlow CK, Nestel PJ, Barnes EH, Kirby A, Thompson P, *et al*. Large-scale plasma lipidomic profiling identifies lipids that predict cardiovascular events in secondary prevention. JCI Insight. 2018; 3: e121326. https://doi.org/10.1172/jci.insight.121326.

[35] Chen Y, Wen S, Jiang M, Zhu Y, Ding L, Shi H, *et al*. Atherosclerotic dyslipidemia revealed by plasma lipidomics on ApoE$^{-/-}$ mice fed a high-fat diet. Atherosclerosis. 2017; 262: 78–86. https://doi.org/10.1016/j.atherosclerosis.2017.05.010.

[36] Xu HM, Huang HL, Liu YD, Zhu JQ, Zhou YL, Chen HT, *et al*. Selection strategy of dextran sulfate sodium-induced acute or chronic colitis mouse models based on gut microbial profile. BMC Microbiology. 2021; 21: 279. https://doi.org/10.1186/s12866-021-02342-8.

[37] Liu X, Zhang Y, Li W, Zhang B, Yin J, Liuqi S, *et al*. Fucoidan Ameliorated Dextran Sulfate Sodium-Induced Ulcerative Colitis by Modulating Gut Microbiota and Bile Acid Metabolism. Journal of Agricultural and Food Chemistry. 2022; 70: 14864–14876. https://doi.org/10.1021/acs.jafc.2c06417.

[38] Zeng Q, Li D, He Y, Li Y, Yang Z, Zhao X, *et al*. Discrepant gut microbiota markers for the classification of obesity-related metabolic abnormalities. Scientific Reports. 2019; 9: 13424. https://doi.org/10.1038/s41598-019-49462-w.

[39] Qiu J, Chen L, Zhang L, Xu F, Zhang C, Ren G, *et al*. Xie Zhuo Tiao Zhi formula modulates intestinal microbiota and liver purine metabolism to suppress hepatic steatosis and pyroptosis in NAFLD therapy. Phytomedicine. 2023; 121: 155111. https://doi.org/10.1016/j.phymed.2023.155111.

[40] Fu T, Huan T, Rahman G, Zhi H, Xu Z, Oh TG, *et al*. Paired microbiome and metabolome analyses associate bile acid changes with colorectal cancer progression. Cell Reports. 2023; 42: 112997. https://doi.org/10.1016/j.celrep.2023.112997.

[41] Chen YC, Bui AV, Diesch J, Manasseh R, Hausding C, Rivera J, *et al*. A novel mouse model of atherosclerotic plaque instability for drug testing and mechanistic/therapeutic discoveries using gene and microRNA expression profiling. Circulation Research. 2013; 113: 252–265. https://doi.org/10.1161/CIRCRESAHA.113.301562.

[42] van Dam AD, Boon MR, Berbée JFP, Rensen PCN, van Harmelen V. Targeting white, brown and perivascular adipose tissue in atherosclerosis development. European Journal of Pharmacology. 2017; 816: 82–92. https://doi.org/10.1016/j.ejphar.2017.03.051.

[43] Chatterjee SB, Dey S, Shi WY, Thomas K, Hutchins GM. Accumulation of glycosphingolipids in human atherosclerotic plaque and unaffected aorta tissues. Glycobiology. 1997; 7: 57–65. https://doi.org/10.1093/glycob/7.1.57.

[44] Summers SA. Could Ceramides Become the New Cholesterol? Cell Metabolism. 2018; 27: 276–280. https://doi.org/10.1016/j.cmet.2017.12.003.

[45] Blüher M, Müller-Wieland D. Editorial: Adipose tissue dysfunction. Frontiers in Endocrinology. 2022; 13: 999188. https://doi.org/10.3389/fendo.2022.999188.

[46] Blüher M. Understanding Adipose Tissue Dysfunction. Journal of Obesity & Metabolic Syndrome. 2024; 33: 275–288. https://doi.org/10.7570/jomes24013.

[47] Wang A, Zhang H, Liu J, Yan Z, Sun Y, Su W, *et al*. Targeted Lipidomics and Inflammation Response to Six Weeks of Sprint Interval Training in Male Adolescents. International Journal of Environmental Research and Public Health. 2023; 20: 3329. https://doi.org/10.3390/ijerph20043329.

[48] Jang HJ, Lim S, Kim JM, Yoon S, Lee CY, Hwang HJ, *et al*. Glucosylceramide synthase regulates adipo-osteogenic differentiation through synergistic activation of PPARγ with GlcCer. FASEB Journal. 2020; 34: 1270–1287. https://doi.org/10.1096/fj.201901437R.

[49] Wang G, Yu Y, Wang YZ, Wang JJ, Guan R, Sun Y, *et al*. Role of SCFAs in gut microbiome and glycolysis for colorectal cancer therapy. Journal of Cellular Physiology. 2019; 234: 17023–17049. https://doi.org/10.1002/jcp.28436.

[50] Yi C, Sun W, Ding L, Yan M, Sun C, Qiu C, *et al*. Short-Chain Fatty Acids Weaken Ox-LDL-Induced Cell Inflammatory Injury by Inhibiting the NLRP3/Caspase-1 Pathway and Affecting Cellular Metabolism in THP-1 Cells. Molecules. 2022; 27: 8801. https://doi.org/10.3390/molecules27248801.

[51] Wang L, Zhang S, Huang Y, Zhou Y, Shan T. Conjugated linoleic acids inhibit lipid deposition in subcutaneous adipose tissue and alter lipid profiles in serum of pigs. Journal of Animal Science. 2023; 101: skad294. https://doi.org/10.1093/jas/skad294.

[52] Zhao X, Oduro PK, Tong W, Wang Y, Gao X, Wang Q. Therapeutic potential of natural products against atherosclerosis: Targeting on gut microbiota. Pharmacological Research. 2021; 163: 105362. https://doi.org/10.1016/j.phrs.2020.105362.

[53] Emoto T, Yamashita T, Sasaki N, Hirota Y, Hayashi T, So A, *et al*. Analysis of Gut Microbiota in Coronary Artery Disease Patients: a Possible Link between Gut Microbiota and Coronary Artery Disease. Journal of Atherosclerosis and Thrombosis. 2016; 23: 908–921. https://doi.org/10.5551/jat.32672.

[54] Duan R, Guan X, Huang K, Zhang Y, Li S, Xia J, *et al*. Flavonoids from Whole-Grain Oat Alleviated High-Fat Diet-Induced Hyperlipidemia *via* Regulating Bile Acid Metabolism and Gut Microbiota in Mice. Journal of Agricultural and Food Chemistry. 2021; 69: 7629–7640. https://doi.org/10.1021/acs.jafc.1c01813.

[55] Antoniades C, Tousoulis D, Vavlukis M, Fleming I, Duncker DJ, Eringa E, *et al*. Perivascular adipose tissue as a source of therapeutic targets and clinical biomarkers. European Heart Journal. 2023; 44: 3827–3844. https://doi.org/10.1093/eurheartj/ehad484.

[56] Shankar K, Kumar D, Gupta S, Varshney S, Rajan S, Srivastava A, *et al*. Role of brown adipose tissue in modulating adipose tissue inflammation and insulin resistance in high-fat diet fed mice. European Journal of Pharmacology. 2019; 854: 354–364. https://doi.org/10.1016/j.ejphar.2019.02.044.

[57] Zhang Y, Dong T, Wang M. Lipidomic landscape of lipokines in adipose tissue derived extracellular vesicles. Frontiers in Molecular Biosciences. 2023; 10: 1281244. https://doi.org/10.3389/fmolb.2023.1281244.

[58] Perdicaro DJ, Rodriguez Lanzi C, Gambarte Tudela J, Miatello RM, Oteiza PI, Vazquez Prieto MA. Quercetin attenuates adipose hypertrophy, in part through activation of adipogenesis in rats fed a high-fat diet. The Journal of Nutritional Biochemistry. 2020; 79: 108352. https://doi.org/10.1016/j.jnutbio.2020.108352.